GEOPHYSICS, VOL. 88, NO. 2 (MARCH-APRIL 2023); P. R135–R143, 8 FIGS.
10.1190/GEO2022-0227.1

Extracting small time-lapse traveltime changes in a reservoir using primaries and internal multiples after Marchenko-based target zone isolation

Johno van IJsseldijk[1], Joost van der Neut[1], Jan Thorbecke[1], and Kees Wapenaar[1]

ABSTRACT

Geophysical monitoring of subsurface reservoirs relies on detecting small changes in the seismic response between a baseline and monitor study. However, internal multiples, related to the over- and underburden, can obstruct the view of the target response, hence complicating the time-lapse analysis. To retrieve a response that is free from the over- and underburden effects, the data-driven Marchenko method is used. This method effectively isolates the target response, which can then be used to extract more precise time-lapse changes. In addition, the method also reveals target-related multiples that probe the reservoir more than once, which further defines the changes in the reservoir. To verify the effectiveness of the method, a numerical example is constructed. This test finds that, when using the isolated target response, the observed time differences resemble the expected time differences in the reservoir. Moreover, the results obtained with target-related multiples also benefit from the Marchenko-based isolation of the reservoir. It is, therefore, concluded that this method has the potential to observe dynamic changes in the subsurface with increased accuracy.

INTRODUCTION

Time-lapse seismic studies are concerned with detecting small changes in the seismic response between a baseline and a monitor study. These changes can either be a difference in amplitude (e.g., Landrø, 2001), a difference in traveltime (e.g., Landrø and Stammeijer, 2004), or a combination of both (e.g., Trani et al., 2011). These time-lapse methods are essential for observing and monitoring subsurface reservoirs, with applications ranging from determining pressure and fluid saturation changes (Landrø, 2001) to monitoring CO_2 injection (Roach et al., 2015) or observing compaction in a reservoir (Hatchell and Bourne, 2005).

In order for these methods to work optimally, it is important that the reservoir response can be clearly identified in the seismic response. In practice, this requirement is not always fulfilled, as multiple reflections from a (highly) reflective overburden can mask the response of the reservoir. It is, therefore, desirable to remove the overburden effects before applying any time-lapse analysis. The Marchenko method can redatum a wavefield from the surface of the earth to an arbitrary focal depth in the subsurface while accounting for all orders of multiples (Slob et al., 2014; Wapenaar et al., 2014). This data-driven method can be used to remove all interactions from layers above the selected focal level, hence giving an unobstructed view of the reservoir response. From this new response, the traveltime difference in the reservoir can more precisely be determined.

In addition to removing the overburden, the reservoir response can be isolated completely by also removing the underburden with the Marchenko method (Wapenaar and Staring, 2018). Consequently, not only the primary response of the reservoir is uncovered, but also internal multiples, which traversed through the reservoir more than once, will now be clearly visible and unobstructed by primaries and multiples outside the target zone. Because these multiples have passed through the reservoir multiple times, the time-lapse traveltime change of the multiples will be larger, hence more sensitive. This is akin to coda-wave interferometry, which exploits the fact that time-lapse changes are exaggerated in the coda due to the longer paths traveled in the medium (Snieder et al., 2002; Grêt et al., 2005).

Inspired by this principle of coda-wave interferometry, Wapenaar and van IJsseldijk (2020) show how the correlation of multiples improves the ability to detect small changes in velocity compared with the correlation of primaries. This method is then adapted to find changes in lateral varying media (van IJsseldijk and Wapenaar, 2021). In this work, we further develop the method to account for time-lapse

Manuscript received by the Editor 21 April 2022; revised manuscript received 23 August 2022; published ahead of production 12 November 2022; published online 27 January 2023.
[1]Delft University of Technology, Department of Geoscience and Engineering, Delft, The Netherlands. E-mail: J.E.vanIJsseldijk@tudelft.nl (corresponding author); j.r.vanderneut@tudelft.nl; J.W.Thorbecke@tudelft.nl; c.p.a.wapenaar@tudelft.nl.

changes in the overburden. First, we revise the theory of isolating the reservoir response with the Marchenko method and review how to extract traveltime changes from this isolated response. Furthermore, we show how multiples traveling through the reservoir can be enhanced to improve the accuracy of the retrieved time shifts. Subsequently, we present a numerical model that will be used to test the methodology. The reservoir response is then isolated from the modeled data, and the traveltime changes of the primary and the multiple reflections are calculated. Finally, we discuss the results and possible future improvements to the method.

THEORY

Time-lapse seismic experiments aim to resolve the differences between a baseline study at a time t_1 and a monitor study conducted at a later time t_2. These differences can be attributed to changes inside of a reservoir and overburden, for example, due to production and geomechanical processes. Here, we propose a method by which the reservoir response is isolated separately for the baseline and monitor studies, after which crosscorrelation between the two studies is used to find the traveltimes differences.

Figure 1 shows the principle of the proposed method. Here, the acoustic situation is considered, with a reservoir enclosed by two strong reflectors. Note how the primary from the first reflector does not probe the reservoir, whereas the primary from the second reflector does. Moreover, the internal multiples generated by these reflectors will traverse the reservoir multiple times; hence, they experience a larger traveltime shift. To achieve this same situation from a regular reflection response measured at the surface, the medium is first divided into three parts: overburden "a," target zone "b," which contains the reservoir and two reflectors as shown in Figure 1, and underburden "c." The reflection response of the full medium is denoted by $R_{abc}(\mathbf{x}_R, \mathbf{x}_S, t)$; here, $\mathbf{x}_R$, $\mathbf{x}_S$, and t denote the receiver position, source position, and time, respectively. Our first aim is to isolate the reflection response R_b of the target zone with the help of the Marchenko method, which will be discussed briefly in the next section.

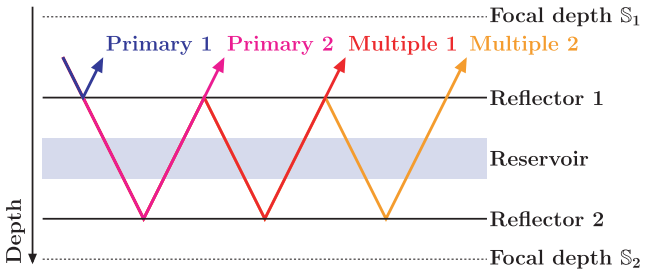

Figure 1. Graphic displaying the principle of the method. Note how the reservoir layer is located in between two reflectors. Primary 1 from reflector 1 does not propagate through the reservoir, whereas primary 2 from reflector 2 does. The multiples (1 and 2) are propagating through the reservoir twice or thrice, hence experiencing double or triple the traveltime changes compared with primary 2. Target zone b is located in between focal depths $\mathbb{S}_1$ and $\mathbb{S}_2$, and overburden a and underburden c are above and below the target zone, respectively.

Extrapolated Marchenko representations

At the base of the Marchenko method are the focusing functions ($f_1^{\pm}$) that allow for retrieval of Green's functions ($G^{-,\pm}$) between the acquisition surface $\mathbb{S}_0$ and a focal level in the subsurface. Here, the left superscript $-$ denotes that the wavefield is upgoing at the receiver position (at the focal level) and the right superscript $\pm$ denotes a down- or upgoing direction from the source position (at the acquisition surface). Van der Neut and Wapenaar (2016) introduce modified functions that are extrapolated to the surface by convolution with the direct arrival of the transmission response (T_d). These extrapolated focusing functions ($v^{\pm}$) are defined as follows:

$$v^{\pm}(\mathbf{x}_R, \mathbf{x}'_S, t) = \int_{\mathbb{S}_F} f_1^{\pm}(\mathbf{x}_R, \mathbf{x}_F, t) * T_d(\mathbf{x}_F, \mathbf{x}'_S, t) d\mathbf{x}_F. \quad (1)$$

Here, $\mathbf{x}_F$ is the coordinate of the focusing point at the focal depth $\mathbb{S}_F$, $\mathbf{x}'_S$ is a coordinate on the acquisition surface, and $*$ denotes temporal convolution. Note that, except for $\mathbf{x}_F$, all coordinates in this work refer to positions at the surface $\mathbb{S}_0$. Similarly, the extrapolated Green's functions ($U^{-,\pm}$) are defined as

$$U^{-,\pm}(\mathbf{x}_R, \mathbf{x}'_S, t) = \int_{\mathbb{S}_F} G^{-,\pm}(\mathbf{x}_R, \mathbf{x}_F, t) * T_d(\mathbf{x}_F, \mathbf{x}'_S, \pm t) d\mathbf{x}_F. \quad (2)$$

These two equations are visualized in Figure 2, which shows how the extrapolated functions are related to the original focusing and Green's functions. By using these extrapolated functions, the retrieved wavefields derived in the next section will be situated at

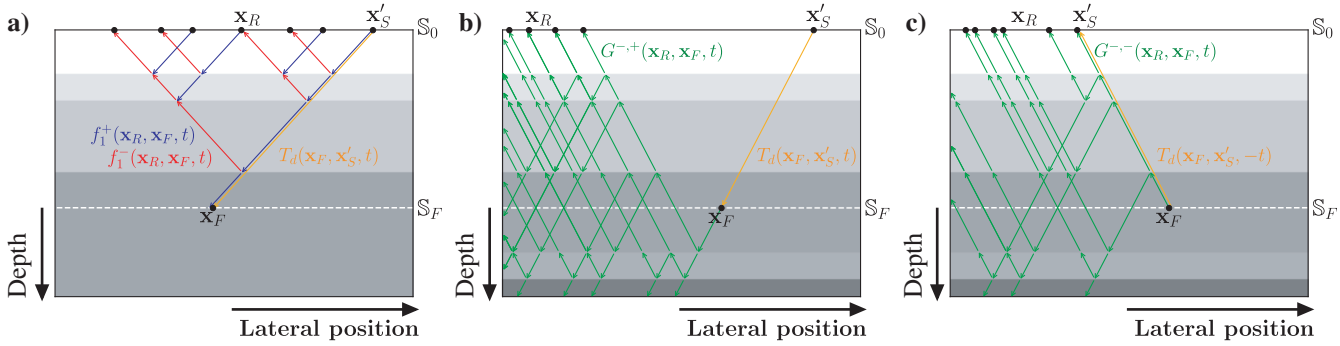

Figure 2. Schematic representation of the extrapolated focusing and Green's functions. (a) The focusing functions f_1^+ (in blue) and f_1^- (in red) are defined in a medium truncated below the focal level ($\mathbb{S}_F$). They are extrapolated to the surface ($\mathbb{S}_0$) using the direct arrival of the transmission response T_d (in orange) to create the extrapolated focusing functions $v^{\pm}$. (b) The downgoing Green's function ($G^{-,+}$) is extrapolated to create $U^{-,+}$. (c) The upgoing Green's function ($G^{-,-}$) creates its extrapolated counterpart $U^{-,-}$.

DOI:10.1190/geo2022-0227.1

the surface $\mathbb{S}_0$ and not at the focal level $\mathbb{S}_F$ as is the case with the regular Marchenko functions. Finally, the same convolutions are applied to the coupled Marchenko representations to find the extrapolated representations:

$$U^{-,+}(\mathbf{x}_R,\mathbf{x}'_S,t)+v^{-}(\mathbf{x}_R,\mathbf{x}'_S,t)=\int_{\mathbb{S}_0}R(\mathbf{x}_R,\mathbf{x}_S,t)*v^{+}(\mathbf{x}_S,\mathbf{x}'_S,t)d\mathbf{x}_S, \tag{3}$$

$$U^{-,-}(\mathbf{x}_R,\mathbf{x}'_S,-t)+v^{+}(\mathbf{x}_R,\mathbf{x}'_S,t)=\int_{\mathbb{S}_0}R(\mathbf{x}_R,\mathbf{x}_S,-t)*v^{-}(\mathbf{x}_S,\mathbf{x}'_S,t)d\mathbf{x}_S. \tag{4}$$

The reflection response is denoted by R. In this paper, this response will either be the response of the full medium R_{abc} or the response after the overburden removal R_{bc}. Moreover, these two equations have four unknowns. To solve this system, a causality constraint is introduced, which exploits the fact that the focusing and Green's functions are separable in time. To apply this constraint, an estimate of the two-way traveltime between the focal level and the surface is required. In our case, this is achieved by computing the direct arrival of the Green's function in a smooth velocity model with an eikonal solver and then convolving this response with itself to find the two-way traveltime. A more elaborate derivation of the Marchenko method is beyond the scope of this paper. Instead, the reader is referred to Wapenaar et al. (2021), who give more background on the regular and extrapolated expressions.

Isolation of the reservoir's response

Using the relations presented in the previous section, the focusing and Green's functions above and below the reservoir can now be retrieved. From these functions, the reflection response of the target zone can be isolated. First, the overburden is removed, using the extrapolated Green's function between the overburden and the upper boundary $\mathbb{S}_1$ of the target zone (Wapenaar et al., 2021):

$$U^{-,+}_{a|bc}(\mathbf{x}_R,\mathbf{x}'_S,t)=-\int_{\mathbb{S}_0}U^{-,-}_{a|bc}(\mathbf{x}_R,\mathbf{x}'_R,t)*R_{bc}(\mathbf{x}'_R,\mathbf{x}'_S,t)d\mathbf{x}'_R. \tag{5}$$

Here, $U^{-,\pm}_{a|bc}$ is the extrapolated Green's functions, retrieved with the Marchenko method from equations 3 and 4, where R_{abc} is used as reflection response R. The vertical line in the subscript indicates the location of the focal level, i.e., between the overburden a and the target-zone b. Equation 5 is solved for R_{bc} by multidimensional deconvolution (MDD) (Wapenaar et al., 2011). This MDD is achieved with least-squares inversion in the frequency domain. Effectively, we have now acquired a new reflection response R_{bc}, which is free from overburden interactions. Furthermore, coordinates $\mathbf{x}'_R$ and $\mathbf{x}'_S$ are located at the surface, due to the use of the extrapolated Green's functions. In contrast, previous work with regular Green's functions have acquired a redatumed response at the focal depth and then required an additional step to extrapolate this response to the surface (van IJsseldijk and Wapenaar, 2021).

Next, the newly acquired reflection response (R_{bc}) is used to retrieve the extrapolated focusing functions between the target zone and the upper boundary $\mathbb{S}_2$ of the underburden. These focusing functions are then used to remove the underburden:

$$v^{-}_{b|c}(\mathbf{x}_R,\mathbf{x}'_S,t)=\int_{\mathbb{S}_0}v^{+}_{b|c}(\mathbf{x}_R,\mathbf{x}'_R,t)*R_b(\mathbf{x}'_R,\mathbf{x}'_S,t)d\mathbf{x}'_R. \tag{6}$$

The subscript $b|c$ denotes that R_{bc} is used to retrieve the focusing functions from equations 3 and 4, with the focal level between target zone b and underburden c. Note that equation 6 directly follows from the definition of the focusing functions in the truncated medium (Wapenaar and Staring, 2018). Again, the reflection response of the target zone R_b can be resolved from equation 6 using MDD.

Effectively, the target zone response has now been isolated, leaving a response analogous to the situation in Figure 1, but with the sources and receivers at the surface $\mathbb{S}_0$. As a final step, the multiples in the final response R_b can be further amplified. First, consider that the multiples in R_b continue infinitely in time, and they are constructed from the focusing functions $v^{-}_{b|c}$ and $v^{+}_{b|c}$, which are finite in time (i.e., they are confined between $t=0$ and the two-way traveltime to the focal depth). Next, $v^{+}_{b|c}$ in equation 6 is divided into an initial function $v^{+}_{b|c,0}$ and a coda $v^{+}_{b|c,m}$ (Wapenaar et al., 2021):

$$v^{+}_{b|c}(\mathbf{x}_R,\mathbf{x}'_R,t)=\delta(\mathbf{x}_{H,R}-\mathbf{x}'_{H,R})\delta(t)+v^{+}_{b|c,m}(\mathbf{x}_R,\mathbf{x}'_R,t). \tag{7}$$

Here, δ denotes the Dirac delta function. From this equation, it follows that the initial function $v^{+}_{b|c,0}$ can be interpreted as a (band-limited) delta pulse at $t=0$. This pulse is followed by the coda $v^{+}_{b|c,m}$. Appendix A shows, when solving equation 6 for R_b, that $v^{+}_{b|c,0}$ is mainly responsible for the primaries in R_b, whereas $v^{+}_{b|c,m}$ updates these primaries and constructs the subsequent multiples of the response. Therefore, by amplifying $v^{+}_{b|c,m}$, the multiples in response R_b should become enhanced as well. Note that this enhancement will cause the amplitudes of the response not to be accurate anymore. However, this is not an issue for the current implementation because only time shifts are desired. Figure 3 shows an overview of the process to isolate the target response. In this chart, only a smooth velocity model of the baseline is used. It is assumed that this model also can be used for the monitor study because the velocity changes are relatively small and only an approximation of two-way traveltime to the focal depth is needed. Next, the new responses R_b for the baseline and monitor will be used to extract the traveltime shifts in the reservoir.

Extraction of time differences

Before extracting the traveltime shifts in the reservoir, the different primaries and multiples are identified. Primary 1 and 2 are easily detected due to the isolation of the target zone (i.e., there are no interactions from the overburden to obscure the primaries). Subsequently, the arrival times of the internal multiples can be approximated based on the primaries, in which the arrival time of the nth multiple can be approximated by the arrival time of primary 2 plus n times the difference in time between the two primaries. The first step is now to eliminate any time shifts resulting from a time-lapse change in the overburden. To do this, the temporal correlation between primary 1 (i.e., the response that is not penetrating the reservoir) and primary 2 or an internal multiple (i.e., the responses that go through the reservoir) is computed. This gives the correlation between primary 1 and the target response below the reservoir:

$$C_*(\mathbf{x}_0,\tau) = \int_0^\infty \Theta_{P1}(t+\tau)R_b(\mathbf{x}_0,t+\tau)\Theta_*(t)R_b(\mathbf{x}_0,t)dt. \tag{8}$$

Here, C is the correlation of the two responses and $\mathbf{x}_0$ denotes the position of the zero-offset traces in the data, where $\mathbf{x}_S = \mathbf{x}_R$. This correlation contains the time lag between the first reflector and P1, M1, or M2. Here, Θ is a time window or mute function that isolates a specific primary or multiple as follows:

$$\Theta_*(t) = \begin{cases} 1, & \text{if } t_* - \epsilon < t \le t_* + \epsilon \\ 0, & \text{otherwise} \end{cases}. \tag{9}$$

In these equations, the asterisk $*$ can be replaced with P1, P2, M1, or M2, for primary 1, primary 2, multiple 1, and multiple 2, respectively. Hence, t_* is the traveltime of one of the primaries or multiples. Here, ϵ is a small constant that defines the window and ensures that the whole waveform is included. Any traveltime differences in the overburden are removed by first calculating the time lag with primary 1 in equation 8, i.e., the time difference between primary 1 and either P2, M1, or M2 is free from overburden interactions. After the time lags of equation 8 have been independently calculated for the baseline and monitor study, the time-lapse traveltime shifts in the reservoir can be determined with a second temporal correlation as follows:

$$\Delta t_*(\mathbf{x}_0) = \arg\max_\tau \left(\int_0^\infty C_*(\mathbf{x}_0,t+\tau)\bar{C}_*(\mathbf{x}_0,t)dt \right). \tag{10}$$

The bar denotes that the monitor correlation is used; thus, the time lags, of primary 2 or one of the multiples with respect to primary 1, for the baseline and monitor are correlated. Next, the argument of the maximum of this correlation is taken to determine the traveltime differences in the reservoir. The process of extracting the time shifts is summarized in Figure 4. Note that there are a few additional practical considerations included in the chart, such as resampling and removing outliers. These will be discussed in more detail in the next section.

NUMERICAL EXAMPLE

A numerical experiment is designed to show the viability of the method. The baseline velocity and density models are shown in Figure 5a and 5b, respectively. Figure 5c displays the change in velocity for the monitor model. In the overburden, there is a velocity decrease of 25 m/s, whereas the velocity and density in the three reservoir compartments increase by 100 m/s and 100 kg/m^3. The reflection responses of the baseline (R_{abc}) and monitor ($\bar{R}_{abc}$) are computed with finite differences, using a wavelet with a flat spectrum between 5 and 80 Hz (Thorbecke and Draganov, 2011). The receivers are placed along a 6000 m long line with a spacing of 10 m, and the data are recorded with a sampling rate of 4 ms. The 601 sources are excited at the same positions as the receivers. Estimates of the two-way traveltimes, between the surface and the focal points at 675 and 1100 m, are acquired using an eikonal solver in a smooth version of the baseline velocity model of Figure 5a. Finally, a band-limited delta pulse is computed, which

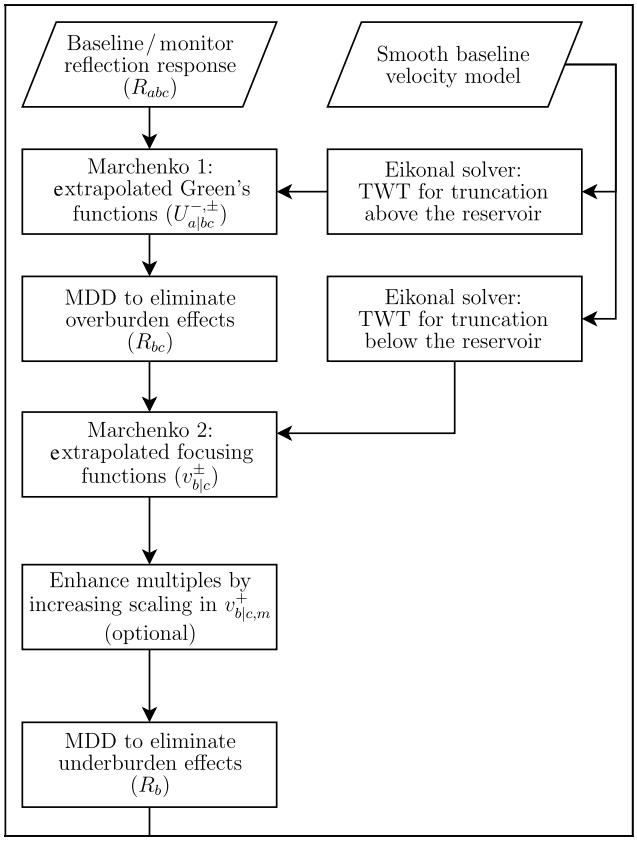

Figure 3. Flowchart depicting how the reservoir response is isolated with the Marchenko method.

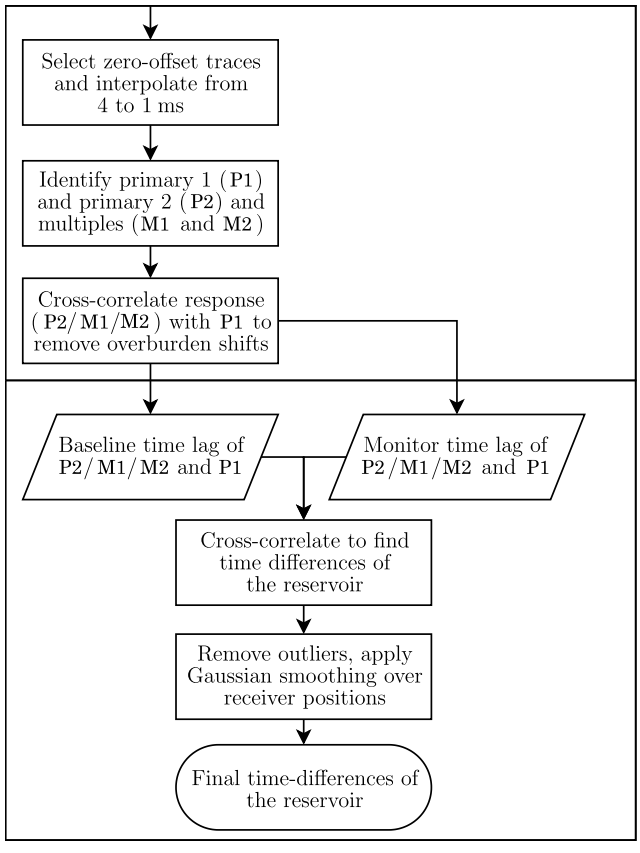

Figure 4. Flowchart depicting how to obtain the time differences in the reservoir from the isolated response (continuation of Figure 3).

DOI:10.1190/geo2022-0227.1

DOI:10.1190/geo2022-0227.1

is used as the initial focusing function (v_0^+) in the iterative Marchenko scheme.

Results of target zone isolation

Figure 6a shows a zero-offset section of the initial reflection response before applying the multiple internal removals (R_{abc}). Note that only the zero-offset data are shown, but the data at all offsets are available and used to compute the isolated reservoir response R_b from R_{abc}. Due to the highly reflective overburden, the primaries (P1 in red and P2 in white) are nearly impossible to identify, and multiple 1 and 2 (in blue and orange) are completely obscured by the overburden and underburden interactions. After removing the overburden and acquiring R_{bc} (Figure 6b), the primaries are now clearly recognizable in the seismogram. However, the windows enclosing the multiples contain undesirable events from primary reflections from the underburden. Figure 6c reveals that these events are successfully removed after the underburden removal. In addition, note how the multiple events are enhanced in Figure 6d. This is the result of the previously described scaling factor applied to $v^+_{b|c,m}$ (which was scaled with a factor of 2.5) before retrieving R_b.

All of the time windows that select the primaries and multiples in Figure 6 are picked from this final response in Figure 6d (R_b). First, the arrival time for both primaries is manually selected. As stated previously, these times are then used to provide an estimate for multiple arrivals. Finally, the windows are manually adjusted to ensure that they include the full response from each individual event. In the next section, these windows will be used for the crosscorrelations that compute the time differences.

Time differences inside the reservoir

From the isolated response, the traveltime changes can be estimated. First, the data are interpolated from 4 to 1 ms to achieve a better time resolution. Second, the primary enclosed in the red window is selected from the data. Similarly, either the second primary, first multiple, or second multiple also is extracted using its respective window (as shown in Figure 6). For the baseline and monitor studies, these responses are then correlated to effectively remove the time differences developed in the overburden, i.e., this correlation retrieves the time lag between P1 and P2, M1, or M2, thus removing the shared path in the overburden. Finally, the baseline and monitor time-lag correlations are mutually correlated to find the time differences in the target zone.

The results of these final correlations are shown in Figure 7. These results can be interpreted as the zero-offset time-lag differences between the baseline and monitor surveys. Hence, any deviation from $\Delta t = 0$ should represent the time shift within the reservoir. Because the velocity in the reservoir is increasing, a negative Δt is expected, whereas a positive shift indicates a velocity decrease (i.e., with the current model, a positive Δt would indicate that the result is contaminated with remaining overburden effects). Note that these results have been acquired with the true Marchenko scaling without the previously described multiple enhancement. Here, the response of the full medium, the response after overburden removal, and the response of the target zone (i.e., after the over- and underburden removal) are displayed with blue, orange, and green lines, respectively. The light-blue area marks the 1D-based zero-offset traveltime difference, which was computed by multiplying two times the reservoir thickness with the slowness change in the reser-

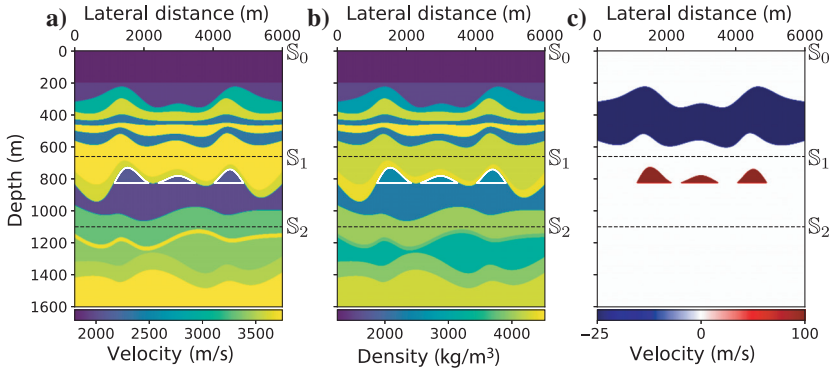

Figure 5. (a) Velocity and (b) density model of the baseline study for the numerical example. The dashed black lines define the focal levels above ($\mathbb{S}_1$) and below the reservoir ($\mathbb{S}_2$), used for the Marchenko method. The solid white contour depicts the three different reservoir pockets. (c) The difference in velocity between the baseline and monitor study. The density inside the reservoir pockets also is increasing with 100 kg/m^3 for the monitor study, with no density changes outside the reservoir. Primary 1 and primary 2 originate from the green-to-blue contrast at 700–900 m and the blue-to-green contrast at 1000 m, respectively.

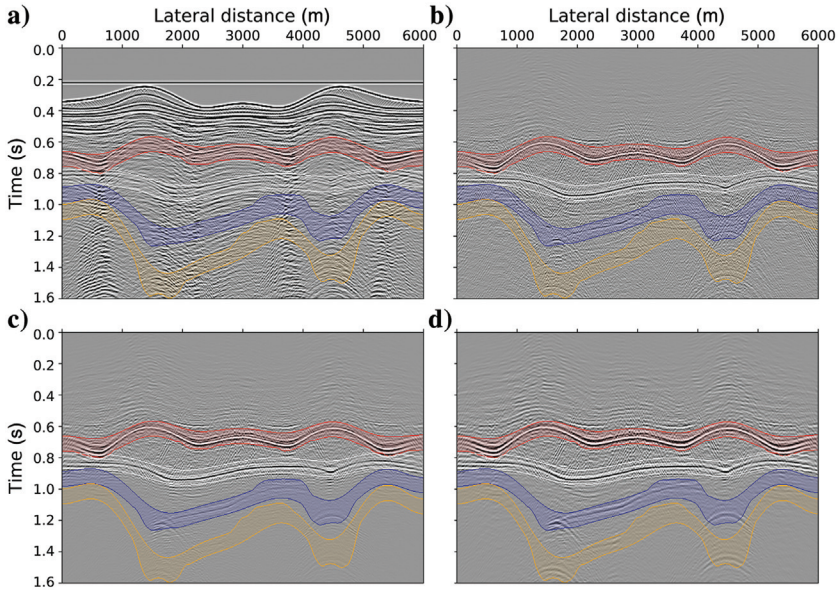

Figure 6. Zero-offset gathers for the baseline reflection response of (a) the entire medium R_{abc}, (b) after the overburden removal R_{bc}, (c) after the over- and underburden removal R_b, and (d) after isolation and multiple enhancement of R_b. The windows used for the crosscorrelation for primary 1, primary 2, multiple 1, and multiple 2 are highlighted in red, white, blue, and orange, respectively.

voir. However, this reference solution does not take into account lateral variations. The red line gives a second reference solution made by cross-correlating "ideal" data. These data have been acquired in a model with a smooth overburden, the same target zone as the actual model, and a transparent underburden. The zero-offset response is then modeled with finite differences, providing an accurate isolated response of the target zone R_b for the monitor and baseline response. Subsequently, the primaries and multiples are identified in the modeled zero-offset response and then correlated as described in the flowchart in Figure 4.

Figure 7a shows the results for primary 2. Although all three responses capture some differences in the reservoir, the response of the full medium still reflects changes in the overburden as shown by the time shifts larger than 0 ms. These positive time shifts are almost fully removed after overburden removal. Note that, on the one hand, the correlations do not match the 1D reference very well, because of the lateral variations in the model. On the other hand, the match with a correlation of the ideal data (the red line) is much better, which implies that the Marchenko-based isolation was successful. Based on these results, it is concluded that the expected time differences are smaller than 15 ms for P1, M1, and M2. This observation is used to achieve more accurate results, by removing outliers that give a time difference larger than 15 ms at any lateral distance (i.e., they are removed before applying the Gaussian smoothing along the lateral direction shown in Figure 4).

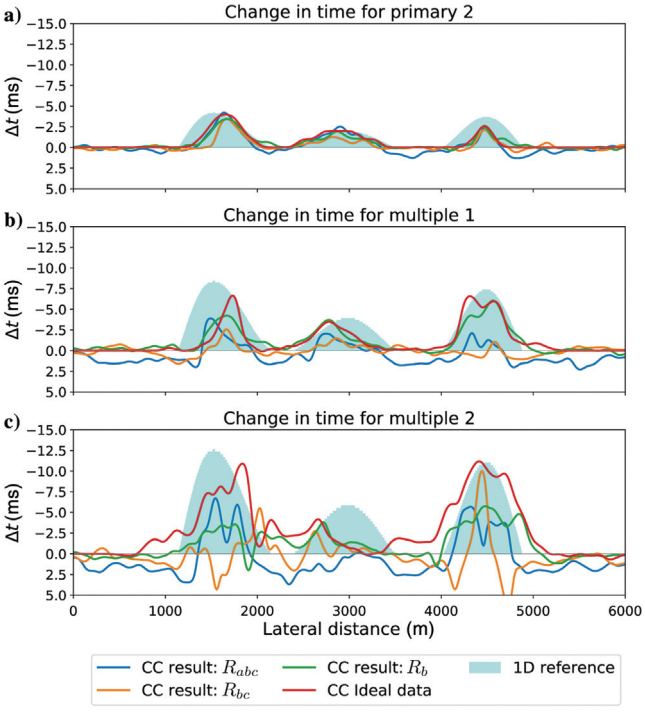

Figure 7. Results showing the estimated time difference in the reservoir from (a) primary 2, (b) multiple 1, and (c) multiple 2; no scaling factor has been applied to enhance the multiples. First, the time lag with primary 1 is computed for the baseline and monitor study. These time lags are then cross-correlated to find the time differences. In each plot, the blue line shows the result derived from the full reflection response (R_{abc}), and the orange and green lines are the time difference derived from R_{bc} and R_b, respectively. The red line shows the crosscorrelations of the ideal data, where R_b is computed using finite differences. The light blue shows the change in time for 1D zero-offset traces (i.e., two times the reservoir thickness times the difference in the slowness).

Next, the procedure is applied to multiples 1 and 2, the results of which are shown in Figure 7b and 7c, respectively. This time, none of the results matches either reference perfectly, and seemingly no meaningful information can be acquired from multiple 2. However, these results are achieved without any multiple enhancement. In the next section, we will explore how the results can be improved by using multiple enhancement.

Results after multiple enhancement

To improve results, i.e., to obtain more accurate time differences, the multiple enhancement is now applied, by scaling $v^+_{b|c,m}$ with a factor of 2.5. This factor is chosen somewhat arbitrarily, but as a general rule, the maximum amplitude in the new $v^+_{b|c,m}$ should not exceed 80% of the maximum amplitude in $v^+_{b|c,0}$. The results of the correlations of this new R_b are shown in Figure 8. The time differences acquired by correlation with primary 2 (Figure 8a) show no significant differences from the original results, but the correlations of the multiples of the isolated response (the green lines in Figure 8b and 8c) match the ideal data (the red lines) much better now. On the contrary, when looking at the results for multiple 1 (Figure 8b), a clear dissimilarity is observed between the results of the isolated response in green and the full response in blue. Furthermore, note the improvement relative to results obtained with primary 2 at a 4500 m lateral distance, where the correlation matches the 1D reference much better. The same can be seen in the results of multiple 2 in

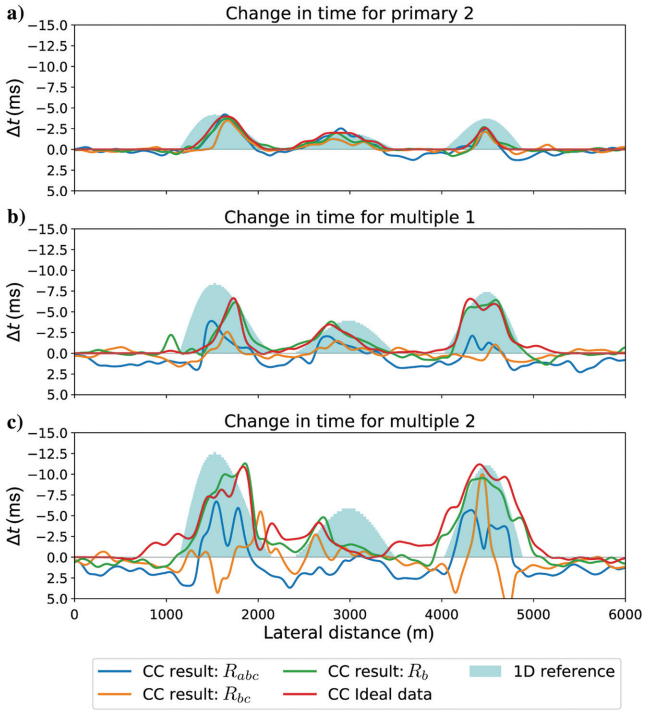

Figure 8. Same results as Figure 7, but with multiple enhancements by applying a scaling factor of 2.5 to $v^+_{b|c,m}$ before retrieving R_b with MDD. Note that the multiple correlations of the isolated response R_b (the green lines in [b] and [c]) are much closer to the ideal result (the red lines) compared with the results without multiple enhancements (Figure 7b and 7c).

DOI:10.1190/geo2022-0227.1

Figure 7c. The two other reservoir compartments at 1500 and 3000 m do not present the same improvements; instead, their results confirm the observations for the correlations with primary 2.

In particular, the results for primary 2 and multiple 1 (the green lines in Figure 8a and 8b) accurately match the correlation of the ideal data. The results of multiple 2 do not have the same match. This is due to the fact that events from multiple 1 are interfering within the correlation window of multiple 2 for the ideal data and leaving an imprint on the reference solution. From this match with the ideal data, it can be concluded that the Marchenko method succeeded in correctly isolating the target response, as the results for multiple 1 coincide with the reference solution. This also highlights the importance of isolating the response because the correlations of the multiples in R_{abc} and R_{bc} do not come close to the reference solution at all. Finally, the results outside the reservoir compartments should show time differences equal to 0 ms, and time differences larger than 0 ms indicate that the result is contaminated by the effects of the overburden. The correlation results of the isolated response R_b display fewer of these positive time differences compared with the results of the full response R_{abc}. Consequently, this is another confirmation that the isolation process has successfully eliminated the effects of the overburden.

DISCUSSION

Although the results show that the reservoir response can be isolated successfully and accurate time differences can be retrieved from the primary reflection and the internal multiples, there are several issues that require a more in-depth discussion. In addition to this discussion, future improvements and practical considerations for the implementation on real data will be considered as well.

First, the scaling factor to $v^{+}_{b|c,m}$, introduced to amplify multiple events, has been found experimentally. The authors have conducted numerous 1D experiments to obtain a better understanding of the effect of the scaling factor and found that the scaled $v^{+}_{b|c,m}$ should not exceed the maximum amplitude in $v^{+}_{b|c,0}$ to maintain a stable result, with as a general rule the amplitudes preferably staying below 80% of this maximum. Due to these nuances, it is always advised to obtain the results without any multiple enhancements first, and only make an effort to improve the results with multiple enhancements after this initial result is achieved.

The second point of discussion is the order of operations used to isolate the target response. In theory, it does not matter whether the underburden is removed before or after overburden removal. Numerical experiments indeed have shown that removing the underburden before the overburden also is a viable approach to isolate the target response, by first retrieving R_{ab} from an MDD of $v^{\pm}_{ab|c}$ and then R_b from $U^{-,\pm}_{a|b}$. However, the previously discussed multiple enhancements are no longer available when the method is applied in this order because the MDD of the focusing functions would be applied before the MDD of the Green's functions that require proper scaling. Therefore, it has been decided to start with overburden elimination followed by the removal of the underburden.

Third, the method is designed to use as little a priori information as possible, needing only three prerequisites: the baseline reflection response (R_{abc}), the monitor reflection response ($\bar{R}_{abc}$), and a smooth version of the baseline velocity model. The smooth velocity model is used to approximate the two-way traveltime between the surface and the focal depth. The same model can be used for the baseline and monitor reflection response because it is assumed that the velocity changes in the medium are relatively small. When the velocity changes are large, a separate velocity model is required to isolate the target zone from the monitor reflection response, but the application of the method would not change otherwise.

In this work, the time shifts are retrieved by a simple crosscorrelation method. Instead of crosscorrelation, a waveform-based or other method could be used to possibly improve the accuracy of the time shift results further. MacBeth et al. (2020) give a comprehensive overview of the different available methods to calculate time shifts.

Next, the primary results before the target zone isolation already match the actual results quite closely, and only minor deviations due to overburden effects are present (i.e., the parts where $\Delta t > 0$ ms). However, these results indirectly benefit from the isolated result because the windows, which are used to identify the primaries, are selected from the isolated results (Figure 6c). Moreover, previous results by van IJsseldijk and Wapenaar (2021) show that the correlations from R_{abc} are insufficient to obtain accurate time differences in less complex models with overburden events interfering with the primaries.

Application of the Marchenko algorithm to field data can be quite cumbersome. In particular, the MDD that is used to remove the overburden effects tends to be very sensitive to errors in the amplitude of the data. To overcome this limitation, Staring et al. (2018) introduce a double-focusing method, which is more stable but leaves some remaining interactions of the overburden. A similar approach is envisioned to acquire R_{bc} when applying this method to real data. It is noted, however, that any errors in R_{bc} will affect the final result of R_b as well. Moreover, the Marchenko method is quite sensitive to incorrect amplitudes in field data. To overcome this limitation, either a scaling factor can be determined using cost functions (Brackenhoff, 2016) or an advanced 3D to 2D conversion can be applied (Dukalski and Reinicke, 2022).

Finally, we would ideally find the velocity change of the reservoir rather than the time differences. For very simple situations, a similar approach to coda-wave interferometry can be considered, which finds the velocity perturbation from the change in traveltime and initial velocity (Snieder, 2006). However, this only holds when the relative velocity perturbation is constant at every location. In our case, the perturbation is different outside the reservoir; hence, the relation does not hold. Alternatively, the velocity perturbation can be found by inversion of crosscorrelations at all offsets (instead of only the zero-offset data used here). Compared with the traveltime differences, the velocity changes can more directly be related to physical processes such as flow in the reservoir. Currently, this is subject to ongoing research.

CONCLUSION

A good understanding of fluid flow, temperature variations, and mechanical changes in subsurface reservoirs is essential for a large variety of geoscientific methods. These dynamic changes can be observed with seismic time-lapse methods by identifying amplitude changes, time shifts, or both between a baseline and a monitor study. However, the response of a subsurface target can be obscured by interferences from reflectors in the overburden and/or underburden, making it more difficult to detect the time-lapse effects. The Marchenko method can be used to remove primaries as well as internal multiples above or below an arbitrary focal level in the subsurface from the reflection response. Hence, this method can be used to isolate the

reservoir response in the baseline and monitor the response, enabling an unobstructed examination of changes in the target zone.

A twofold methodology has been proposed to extract time differences. With this methodology, first, the target response is isolated by overburden removal, followed by underburden removal. This new response is then used to identify the primary and multiple reflections in the target zone. Second, time differences are retrieved by cross-correlating the different reflections of the baseline and monitor studies. By first correlating the response with primary 1 above the reservoir, all possible time shifts of the overburden are removed.

A numerical example with a strongly reflective overburden was created to test the methodology. The isolation of the target zone revealed the primary responses of the reservoir, allowing their extraction from the data. Next, the time differences of the reservoir could be approximated from correlations with a primary reflection below the reservoir. Furthermore, additional traveltime changes were retrieved from the first- and second-order multiples, created by the two reflectors enclosing the reservoir. These multiples confirmed the earlier observations but also improved specific blind spots in the original approximation of the time changes.

The proposed methodology provides a new means to extract traveltime differences, especially for situations in which complex overburden and underburden interactions mask the target response. Future developments also should make it possible to invert for velocity changes in the reservoir rather than time differences. The method will then enable us to more accurately observe dynamic changes in the subsurface.

ACKNOWLEDGMENTS

The authors are grateful for the insightful comments of Qiang Guo and two anonymous reviewers. We also thank L. Diekmann, G. Meles, M. Staring, and J. Brackenhoff for insightful discussions about this work. This research was funded by the European Research Council (ERC) under the European Union's Horizon 2020 research and innovation program (grant agreement no. 742703).

DATA AND MATERIALS AVAILABILITY

Data associated with this research are available and can be accessed via the following URL: https://gitlab.com/geophysicsdelft/OpenSource. The figures in this paper can be reproduced using the demo in the "vmar" folder of the repository.

APPENDIX A

MULTIPLE ENHANCEMENT

This appendix aims to give a more comprehensive explanation as to why increasing the weight of $v^+_{b|c,m}$ results in enhanced multiples in the final reflection response R_b. The first operator $\mathcal{V}^+_m$ is defined to apply a multidimensional convolution with $v^+_{b|c,m}$, as follows:

$$\mathcal{V}^+_m R_b(\mathbf{x}_R, \mathbf{x}'_S, t) = \int_{\mathbb{S}_0} v^+_{b|c,m}(\mathbf{x}_R, \mathbf{x}'_R, t) * R_b(\mathbf{x}'_R, \mathbf{x}'_S, t) d\mathbf{x}'_R. \tag{A-1}$$

Next, this equation and equation 7 are substituted in equation 6. After rearranging the terms, an expression to obtain R_b is acquired:

$$R_b(\mathbf{x}_R, \mathbf{x}'_S, t) = (1 + \mathcal{V}^+_m)^{-1} v^-_{b|c}(\mathbf{x}_R, \mathbf{x}'_S, t). \tag{A-2}$$

Finally, the inverse in equation A-2 can be expanded as a Neumann series:

$$R_b(\mathbf{x}_R, \mathbf{x}'_S, t) = \sum_{k=0}^{\infty} (-\mathcal{V}^+_m)^k v^-_{b|c}(\mathbf{x}_R, \mathbf{x}'_S, t). \tag{A-3}$$

Equation A-3 illustrates how the primaries and multiples in R_b are constructed from the focusing functions. First, for $k = 0$, only the contributions from $v^-_{b|c}$ are available. This will account for the primaries and multiples contained in R_b from times $t = 0$ up to times below the two-way traveltime to the focal depth because $v^-_{b|c}$ is equal to zero outside this range. Consequently, the multiples at times larger than the two-way traveltime have to be constructed from terms with $k > 0$, which will be created using $v^+_{b|c,m}$. This implies that the multiples in R_b can be enhanced artificially by amplifying $v^+_{b|c,m}$. Application of equation A-3 is only stable if the L2 norm of the operator is less than one, i.e., $\|\mathcal{V}^+_m\|_2^2 < 1$. This constraint does not necessarily hold for all subsurface models. Because of this limitation, the Neumann series is solely introduced here to provide an intuitive explanation for the multiple enhancement, whereas the MDD in equation 6 is solved by least-squares inversion in the frequency domain.

REFERENCES

Brackenhoff, J., 2016, Rescaling of incorrect source strength using Marchenko redatuming: M.S. thesis, TU Delft repository, Delft University of Technology.

Dukalski, M., and C. Reinicke, 2022, Marchenko multiple elimination using conventional vs advanced 3-D to 2-D conversion on marine data: 84th Annual International Conference and Exhibition, EAGE, Extended Abstracts, doi: 10.3997/2214-4609.202210182.

Grêt, A., R. Snieder, R. C. Aster, and P. R. Kyle, 2005, Monitoring rapid temporal change in a volcano with coda wave interferometry: Geophysical Research Letters, **32**, L06304, doi: 10.1029/2004GL021143.

Hatchell, P. J., and S. J. Bourne, 2005, Measuring reservoir compaction using time-lapse timeshifts: 75th Annual International Meeting, SEG, Expanded Abstracts, 2500–2503, doi: 10.1190/1.2148230.

Landrø, M., 2001, Discrimination between pressure and fluid saturation changes from time-lapse seismic data: Geophysics, **66**, 836–844, doi: 10.1190/1.1444973.

Landrø, M., and J. Stammeijer, 2004, Quantitative estimation of compaction and velocity changes using 4D impedance and traveltime changes: Geophysics, **69**, 949–957, doi: 10.1190/1.1778238.

MacBeth, C., H. Amini, and S. Izadian, 2020, Review paper: Methods of measurement for 4D seismic post-stack time shifts: Geophysical Prospecting, **68**, 2637–2664, doi: 10.1111/1365-2478.13022.

Roach, L. A. N., D. J. White, and B. Roberts, 2015, Assessment of 4D seismic repeatability and CO_2 detection limits using a sparse permanent land array at the Aquistore CO_2 storage site: Geophysics, **80**, no. 2, WA1–WA13, doi: 10.1190/geo2014-0201.1.

Slob, E., K. Wapenaar, F. Broggini, and R. Snieder, 2014, Seismic reflector imaging using internal multiples with Marchenko-type equations: Geophysics, **79**, no. 2, S63–S76, doi: 10.1190/geo2013-0095.1.

Snieder, R., 2006, The theory of coda wave interferometry: Pure and Applied Geophysics, **163**, 455–473, doi: 10.1007/s00024-005-0026-6.

Snieder, R., A. Grêt, H. Douma, and J. Scales, 2002, Coda wave interferometry for estimating nonlinear behavior in seismic velocity: Science, **295**, 2253–2255, doi: 10.1126/science.1070015.

Staring, M., R. Pereira, H. Douma, J. van der Neut, and K. Wapenaar, 2018, Source-receiver Marchenko redatuming on field data using an adaptive double-focusing method: Geophysics, **83**, no. 6, S579–S590, doi: 10.1190/geo2017-0796.1.

Thorbecke, J. W., and D. Draganov, 2011, Finite-difference modeling experiments for seismic interferometry: Geophysics, **76**, no. 6, H1–H18, doi: 10.1190/geo2010-0039.1.

Trani, M., R. Arts, O. Leeuwenburgh, and J. Brouwer, 2011, Estimation of changes in saturation and pressure from 4D seismic AVO and time-shift analysis: Geophysics, **76**, no. 2, C1–C17, doi: 10.1190/1.3549756.

van der Neut, J., and K. Wapenaar, 2016, Adaptive overburden elimination with the multidimensional Marchenko equation: Geophysics, **81**, no. 5, T265–T284, doi: 10.1190/geo2016-0024.1.

van IJsseldijk, J., and K. Wapenaar, 2021, Discerning small time-lapse traveltime changes by isolating the seismic response of a reservoir using the Marchenko method: First International Meeting for Applied Geoscience & Energy, SEG, Expanded Abstracts, 3449–3453, doi: 10.1190/segam2021-3583007.1.

Wapenaar, K., J. Brackenhoff, M. Dukalski, G. Meles, C. Reinicke, E. Slob, M. Staring, J. Thorbecke, J. van der Neut, and L. Zhang, 2021, Marchenko redatuming, imaging, and multiple elimination and their mutual relations: Geophysics, **86**, no. 5, WC117–WC140, doi: 10.1190/geo2020-0854.1.

Wapenaar, K., and M. Staring, 2018, Marchenko-based target replacement, accounting for all orders of multiple reflections: Journal of Geophysical Research: Solid Earth, **123**, 4942–4964, doi: 10.1029/2017JB015208.

Wapenaar, K., J. Thorbecke, J. van der Neut, F. Broggini, E. Slob, and R. Snieder, 2014, Marchenko imaging: Geophysics, **79**, no. 3, WA39–WA57, doi: 10.1190/geo2013-0302.1.

Wapenaar, K., J. van der Neut, E. Ruigrok, D. Draganov, J. Hunziker, E. Slob, J. Thorbecke, and R. Snieder, 2011, Seismic interferometry by crosscorrelation and by multidimensional deconvolution: A systematic comparison: Geophysical Journal International, **185**, 1335–1364, doi: 10.1111/j.1365-246X.2011.05007.x.

Wapenaar, K., and J. van IJsseldijk, 2020, Employing internal multiples in time-lapse seismic monitoring, using the Marchenko method: 82nd Annual International Conference and Exhibition, EAGE, Extended Abstracts, doi: 10.3997/2214-4609.202011576.

Biographies and photographs of the authors are not available.